Using seismic and CSEM imaging to improve geological understanding of mineralisation along Mohns Ridge

Vetle Vinje[1]*, Marit Stokke Bauck[1], Hao Jiang[1], Carsten Scholl[1], Stephen Edwards[1], Sarah Hill[1], Federico Buriola[1] and Richard Wombell[1] study the use of 2D seismic and controlled source electromagnetic (CSEM) data to image the subsurface geology of the Mohns Ridge segment of the Arctic Mid-Ocean Ridge.

Introduction

It is now widely recognised that seafloor metal-bearing mineral deposits, namely the big three of manganese nodules, ferromanganese crusts, and seafloor massive sulphides (SMSs) and their associated sediments, host many of the elements (e.g., cobalt, copper and nickel) essential to reducing societal reliance on fossil fuels as a part of the energy transition. Consequently, it has become urgent to find and better understand these deposits, evaluate their metal potential, and quantify the risks associated with their extraction.

In the case of SMSs, they are associated with submarine volcanically active tectonic plate boundaries and, therefore, are present along many segments of the world's mid-ocean ridge (MOR), volcanic arc and back-arc spreading systems. They form at and below the seabed, morphologically exposed at the surface as mounds, vents and chimneys, where warm hydrothermal fluids vent into cold ocean-bottom water (Edmonds et al., 2003). In size, they typically reach up to a few hundred metres in lateral extent (Murton et al., 2019). Venting occurs along all MORs (about 60,000 km in total length), regardless of spreading rate, and SMS bodies become larger and more widely spaced as spreading rate decreases, leading to an estimate that 85% of the total tonnage of SMS deposits at MORs may occur where spreading rates are slow to ultraslow (e.g., Hannington et al., 2011; German et al., 2016). Furthermore, surface samples of SMSs collected from several slow and ultraslow spreading locations have yielded some of the highest average concentrations of copper (>10% by weight) for the global MOR system (German et al., 2016).

The quality of exploration for SMS deposits will continue to improve as more becomes known about their geological setting, both at the surface and in the subsurface. In this work, we have studied the surface morphology and subsurface geology of the Mohns Ridge segment of the ultraslow-spreading Arctic Mid-Ocean Ridge (Figure 1), including the areas adjacent to the SMS bodies known as Mohns Treasure. Surface morphology was imaged using bathymetry, but our main contribution was to evaluate imaging of the shallow subsurface (i.e., the first kilometre or so) using both two-dimensional (2D) seismic and controlled source electromagnetic (CSEM) data. This included evaluating the improvements in both seismic acquisition, processing and imaging by comparing a 2D vintage seismic survey from 2001 with a recent 2D acquisition from 2022. In the context of the Mohns Treasure SMS deposit, we investigated the potential of seismic and CSEM to identify and improve the geological understanding of this mineralised zone.

Study area, data acquisition and methods

Mohns Ridge has been the subject of academic studies for the past 60 years and several data acquisition campaigns have been conducted, including those for bathymetry and multi-year 2D seismic data starting in the late Sixties (Talwani and Eldholm, 1977). These have revealed that the plate boundary has a complex morphology, rifting and spreading history (Bruvoll et. al., 2009, and references therein). Mohns Ridge is in deep water (2000-3500 m) and is an ultraslow-spreading ridge (Johansen et al., 2019). It hosts potentially significant resources (Ressursvurdering havbunnsmineraler, 2023) of SMS deposits containing copper, zinc, gold, silver, and cobalt. The Norwegian government announced in 2022 its intention to open areas over the Arctic Mid-Ocean Ridge for mineral exploration and, subsequently, deep-sea mining (Press Release, 2023).

A significant SMS discovery was Mohns Treasure in 2002 at a water depth of 2600 m during dredging of the seafloor (Pedersen et al., 2010). Chimney fragments were retrieved from a ledge left behind after mass wasting from the inner wall of the north-western flank of the rift valley where Mohns Treasure is located (red star in Figure 2). These authors suggested that the hosting sediments likely represent the outer parts of the Bear Island fan that originally accumulated in the rift valley before being uplifted during marginal faulting and subsequently failing through mass movement.

The data sets used in this study come from two surveys (Figures 1 and 2). The first is the Svalex 2D seismic survey undertaken in 2001 as part of a student programme organised by the University

[1] CGG
* Corresponding author, E-mail: vetle.vinje@cgg.com
DOI: 10.3997/1365-2397.fb2023087

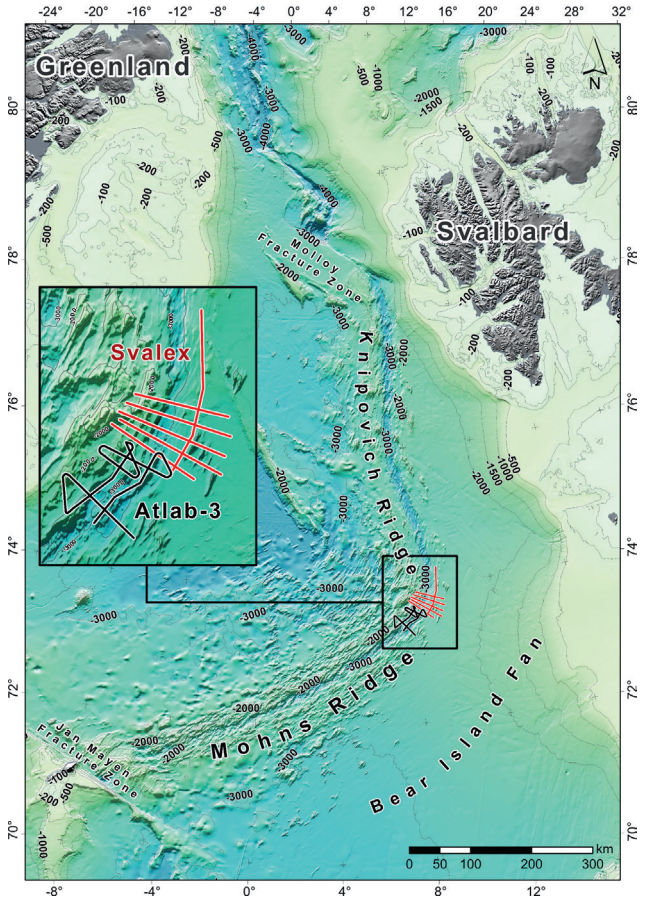

Figure 1 Regional bathymetric map of the Mohns and Knipovich Ridges which are part of the Arctic Mid-Ocean Ridge in the Western part of the Norwegian Sea with the two exploration surveys: Svalex from 2001 in red and Atlab-3 from 2022 in black.

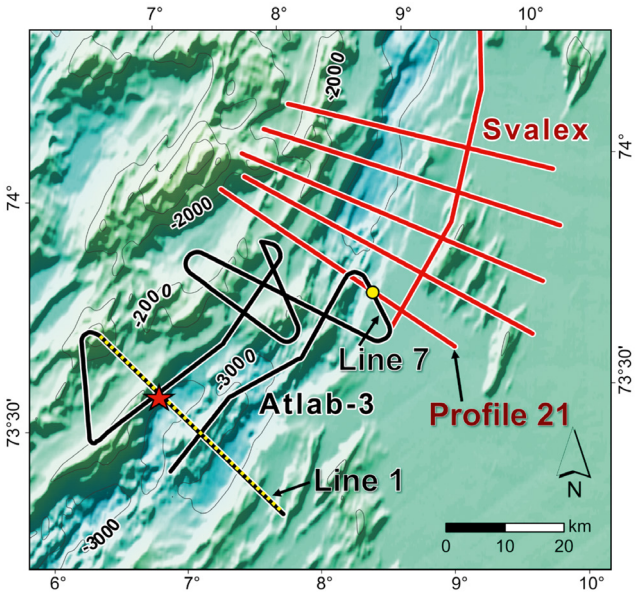

Figure 2 Zoom of the survey area in the northern part of Mohns Ridge showing the locations of the Svalex Profile 21 and Atlab Line 7 intersecting in the yellow circle and the Atlab Line 1 where seismic-constrained CSEM inversion was performed. Mohns Treasure is indicated by a red star.

of Bergen. This survey consisted of five seismic profiles across the Mohns-Knipovich bend and one profile along the ridge.

The second set of data was acquired as part of the Atlab-3 project led by the ATLAB consortium organised by the Norwegian University of Science and Technology (NTNU). Earlier phases of the ATLAB project focused on controlled source electromagnetic (CSEM) and magnetotelluric (MT) methods (Johansen, et al. 2019). In 2022, Phase 3 of ATLAB (Atlab-3) acquired 2D seismic, CSEM and MT data, as well as measurements from the deep-sea environment. A total of eight lines of 2D seismic were shot in Atlab-3, both parallel and perpendicular to the spreading axis. Along Line 1 of Atlab-3 (Figure 2), a 2D CSEM with 23 CSEM sea bottom nodes were acquired in addition to the 2D seismics. This line passes close to Mohns Treasure.

Seismic imaging

Table 1 lists the seismic acquisition parameters of the Svalex and Atlab-3 surveys. The source volume and streamer length were considerably larger on the Svalex survey compared to the Atlab-3 survey, although the Atlab-3 survey had higher fold due to the smaller source increment. The Atlab-3 survey also benefited from a deeper streamer depth enabled by the dual-sensor streamer (Carlson et al., 2007) and included the recording of the source signature using a near-field hydrophone located about 1 m above the two airguns.

The availability of this seismic data gives us the opportunity to compare migrated seismic lines over the northern part of Mohns Ridge. These are:

(i) the Svalex data on Profile 21 (Figure 2) from 2001, processed in 2003 (Bruvoll et al., 2009). The processing sequence was standard for the time and consisted of band-pass filtering, NMO correction and DMO (Dip-moveout), stacking and poststack migration.

(ii) the same 2001 Svalex data from Profile 21, processed in 2023 using state-of-the-art processing and imaging technologies consisting of denoising, source designature based on water bottom reflections, source and receiver deghosting and pre-stack time migration, stacking and low-pass filtering.

(iii) the modern 2022 Atlab-3 data (Figure 2), where the processing utilised the near-field hydrophones in the source designature and the dual-sensor recording in the streamer to

	Svalex (2001)	Atlab-3 (2022)
Seismic vessel	Håkon Mosby (University of Bergen)	M/V Atlantic Guardian (EMGS)
Source volume	776 cu in	90 cu in (2x45 cu in)
Source depth	10 m	5 m
Source increment	50 m	12.5 m
Smallest offset	112.5 m	50 m
Streamer length	3000 m	1200 m
Streamer depth	7 m	18 m
Sensor type	Hydrophone	Hydrophone and geophone
Receiver spacing	12.5 m	12.5 m
Sampling interval	2 ms	2 ms
Fold	30	48

Table 1 Survey parameters of the Svalex (2001) and Atlab-3 (2022) 2D surveys.

perform receiver-side deghosting (Carlson et al., 2007). The source ghost was then attenuated, followed by a standard processing and imaging workflow as described in (ii).

The water depth ranges between ~1600 m to more than 3000 m so there was no need to perform demultiple as the water-bottom multiple arrives below the area of interest. Due to the side scattering in the 2D lines it was also not possible to use the RMO (Residual-moveout) in image gathers to estimate the migration velocities. Instead, sparse regional velocities were used as an initial model followed by migration velocity scans.

Profile 21 is the southernmost line in the Svalex data crossing the Mohns Ridge perpendicularly, as shown in Figure 2. Time-migrated images of the profile are shown in Figure 3 with the vintage processing from 2003 (top) and the latest state-of-the-art processing and imaging from 2023 (bottom).

The south-eastern part of the line is dominated by the Bear Island Fan with a sediment package that is up to 800 m thick. Close to the centre of Mohns Ridge is the Axial Volcanic Ridge (AVR) with symmetrical valleys immediately on each side. The western part of the profile is dominated by rotated fault blocks partly filled with sediments. The sediments in blocks annotated A to E in Figure 3 have been tilted by the faulting and dragged along the fault footwall causing the folding. The upper sediments are less tilted and may represent debris off emerging fault scarps.

The seismic quality in the irregular basaltic structures, ridges and blocks close to the AVR is poor on both images. The Svalex data is 2D which means that the imaging process will move out-of-plane reflections into the 2D image plane creating a large number of uncollapsed events and misplaced energy. This is particularly visible in the AVR and the surrounding valleys where even the

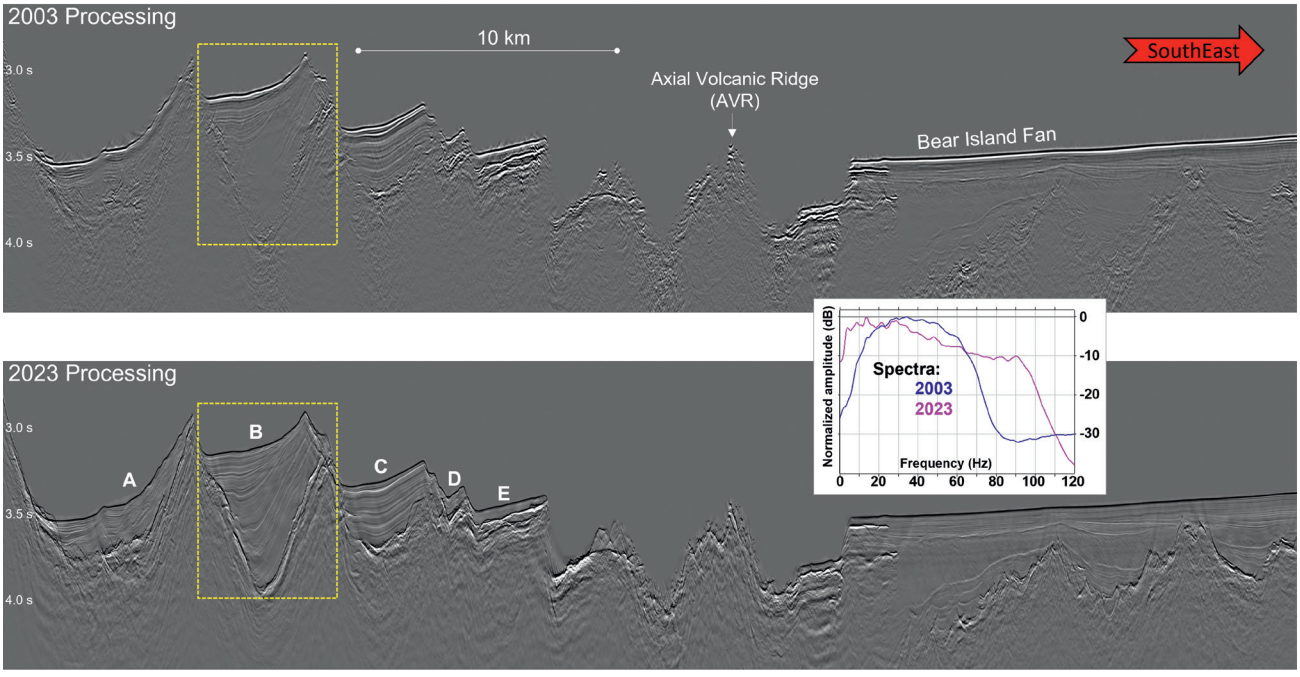

Figure 3 Profile 21 of the Svalex data across Mohns Ridge including the central Axial Volcanic Ridge with legacy processing from 2003 (top) and modern state-of-the art processing from 2023 (bottom) with rotated fault blocks A to E.

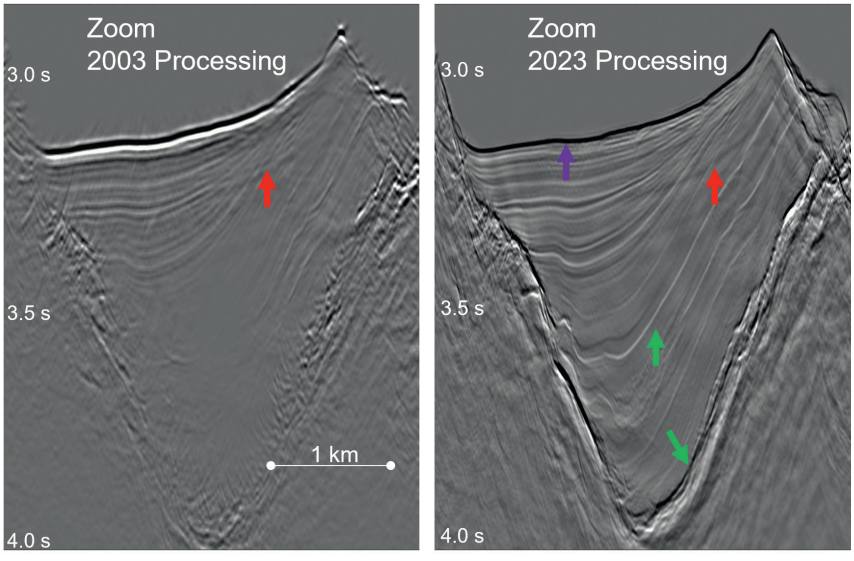

Figure 4 Zoom of a sedimentary basin in the Svalex Profile 21 in the yellow dashed rectangles in Figure 3. Red arrows represent residual bubble energy, the purple arrow indicates the water bottom, and the green arrows depict sedimentary layers and the bottom of the basin.

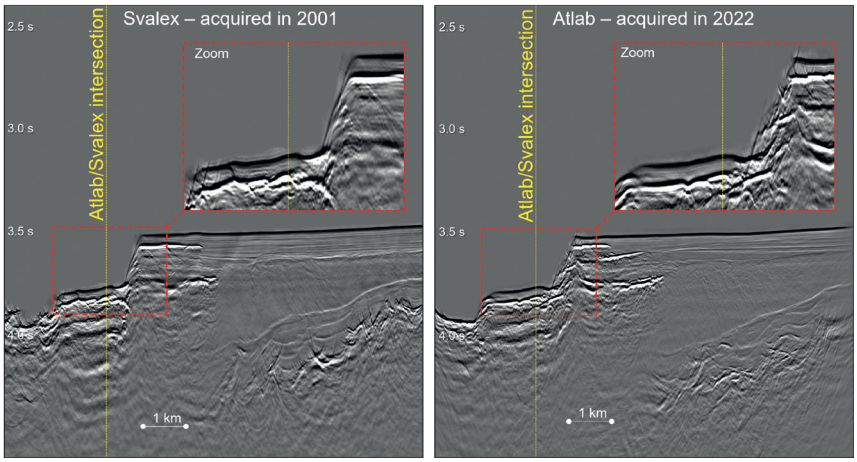

Figure 5 Intersecting 2D seismic lines of Svalex Profile 21 (left) and Atlab-3 Line 7 (right) from the 2023 state-of-the-art processing with a flat abyssal plane to the east and two faulted blocks to the west towards the AVR.

water bottom is imaged as a chaotic mess. However, in areas with less off-plane variation in the geology, decent imaging is achieved. There is a significant improvement in image quality in the 2023 processing compared to the 2003 processing, as expected. The imaging in the fine layering in sedimentary basins is much better, the overall bandwidth is wider, and the wavelet is zero-phased, as seen from the phase of the reflectors, especially the water bottom.

Figure 4 shows a zoom of a sedimentary basin about 15 km west of the AVR indicated by the dashed yellow rectangles in Figure 3. There is improved sedimentary layering and base (green arrows), improved signal phase of the water bottom (purple arrow) and a sharper and more broadband appearance in the modern profile on the right. Due to the lack of near-field hydrophones close to the airgun source array in the vintage Svalex acquisition it was a challenge to remove the bubble energy from the data. A residual bubble hanging from the water bottom is indicated by the red arrow on both images in Figure 4.

Figure 5 shows a comparison of about 10 km of the 2D images from the vintage Svalex data (left) and the modern Atlab-3 data Line 7 (right).

As seen in the map in Figure 2, Atlab-3 Line 7 intersects with Svalex Profile 21 as indicated by the yellow circle. The geology is identical between the lines in this intersection (yellow dotted line in Figure 5). Both data sets have been processed and imaged in 2023 using the workflows described above. The image quality is comparable, but, as seen from the low-frequency wobbles in the Svalex spectrum in Figure 6, the Svalex data is partly contaminated by residual bubble energy and has less high-frequency energy above ~90 Hz. It is remarkable that the small-volume source of the Atlab-3 acquisition of only ~10% of the Svalex acquisition source (Table 1) does not reduce the penetration depth of the imaging. It is also an advantage for processing to have near-field source measurements and a multi-sensor streamer present in the Atlab-3 acquisition as this can help to solve the bubble and receiver ghost problems.

Figure 9 shows the seismic image for Atlab-3 Line 1 co-rendered with the bathymetry of the sea bottom and the vertical resistivity derived from the CSEM inversion, which is described in the next section. The 2D seismic data in Line 1 was processed and imaged using the same workflow as for Line 7 farther north (Figure 5, right). A single seismic sea-bottom node indicated in Figure 8 was located about 5 km south-east of the AVR and welded to one of

Figure 6 Frequency spectra of the two lines in Figure 5 showing comparable low-frequency content but the slightly higher frequencies of the Atlab data. Notice the wobbling in the <15 Hz part of the Svalex spectrum caused by residual source bubble.

the EM nodes at a depth of 3126 m. The data quality of this seismic node was excellent, especially for the low frequencies of less than 8 Hz. It was used to estimate the water velocity (V_w=1477.6 m/s) for the seismic imaging with a traveltime-based inversion procedure based on the direct wave traveltimes from the airgun sources in the 2D seismic lines of Atlab-3.

CSEM imaging

In addition to the seismic data, CSEM data was also acquired along Atlab-3 Line 1 which runs close to the known SMS deposit called Mohns Treasure indicated in the map in Figure 2. A total of 23 CSEM nodes were deployed on the seabed in depths ranging from 1660 to 3140 m (Figures 7 and 8). The nominal spacing of the nodes was 2000 m but the actual spacing was quite irregular due to the rough topography of the seabed. The *Atlantic Guardian* vessel operated by EMGS which acquired the seismic data was also used to tow the EM source. The EM source was a transmitter dipole transmitting a signal with a base frequency of 0.5 Hz. It was towed as close to the seabed as possible but, due to the rough topography, the distance from the EM source to the seabed ranged from about 35 m to more than 800 m, as can be seen in Figure 8.

The CSEM data was inverted with a finite-difference-based inversion method (Scholl and Miorelli, 2019). The inversion used the data for the frequencies 0.5, 1, 2 and 3.5 Hz with offset

ranges between 1500 m to 11 km. As part of comprehensive testing, multiple inversions were run assuming a vertical transverse isotropic (VTI) resistivity. These tests included inversions on 2D and 3D models, based on either the electric Ex or the magnetic Hy component or both.

Two factors related to the steep and irregular bathymetry are expected to reduce the near-surface resolution and stability of the inversion: (i) the large distance from the transmitter dipole to the seafloor, as shown in Figure 8, and (ii) the uncertainty in the position and orientation of the receiver antennas of the CSEM nodes. Despite this, the results were generally similar between the various inversions. Figure 9 shows the result in the shallow region beneath the water bottom obtained using the Hy data only. The vertical resistivity model was obtained using the seismic section as a structural guide (Scholl et al., 2017) via the cross-gradient method (Gallardo and Meju, 2003). Given that the seismic data is available only along a 2D line, this approach could only be reasonably used in a 2D CSEM inversion.

Discussion

The asymmetry of Mohns Ridge either side of the AVR is clearly evident in both Figures 3 and 9, showing that the north-western side of the ridge is more elevated and rugged than the largely flatter and sediment-covered south-eastern flank. This is consistent with an ultraslow-spreading zone where extension is driven by weak magmatic and more dominant tectonic processes (e.g., Buck et al., 2005). In Figure 3, sediments of the Bear Island fan are sub-horizontal and reach a thickness of 800 m. In contrast, sediments on the north-western flank of the ridge have been rotated counterclockwise during faulting (Figure 3), again emphasising the asymmetry across the whole ridge system. The folding pattern in some sediments in the north-west (Figure 4) suggests that they were dragged along the footwall as they were tilted. The upper sediments are less tilted and deformed and may represent accumulated debris off emerging fault scarps.

In slow to ultraslow spreading zones, detachment faulting dominates the tectonic process and drives crustal thinning and exposure of lower crustal and upper mantle lithologies in oceanic core complexes (e.g., Canales and Escartín, 2010). It also plays an important role in fluid migration and formation of SMS deposits, of which Mohns Treasure is an example. Pedersen et al. (2010) first showed the close relationship between Mohns Treasure and a low-angle fault zone, and Lim et al. (2019) re-emphasised the association and major rift-forming faults acting as important fluid pathways. Large faults and fault scarps are clearly evident in Figures 3 and 9 and may be associated with the detachment process. Importantly, they are adjacent to Mohns Treasure and may, therefore, represent fluid pathways linked to the mineralisation. In the resistivity there is a tilted and elongated area of low resistivity a few hundred metres underneath Mohns Treasure, which could be an indication of high fluid saturation.

In the CSEM results (Figure 9), the AVR has a moderate resistivity consistent with porous volcanic material, while the rift valleys on each side, with more consolidated material, show large pockets of high resistivity indicating lower pore volume. We also observe lower resistivity in the sedimentary packages on plateaus to the east and west in the section, which is expected.

Key components of the mineralising system at Mohns Treasure are indicated, specifically the juxtaposition of major faults and a zone of potentially high fluid saturation in Figure 9, although the actual SMS bodies do not appear to be directly imaged. This is probably due to the 2D limitations of the acquisition, as the seismic line does not appear to track exactly over Mohns Treasure which is probably only a few 100 m in size and the water-bottom is poorly

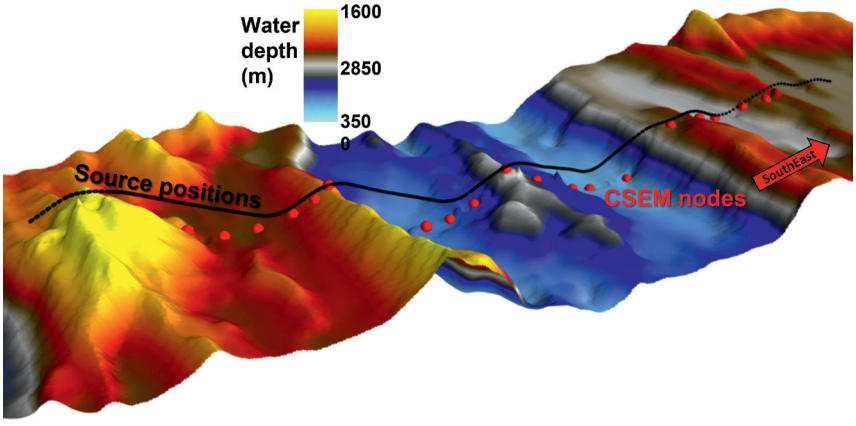

Figure 7 Bathymetry along Line 1 showing the position of the CSEM receiver nodes (red) and the track of the transmitter dipole (black).

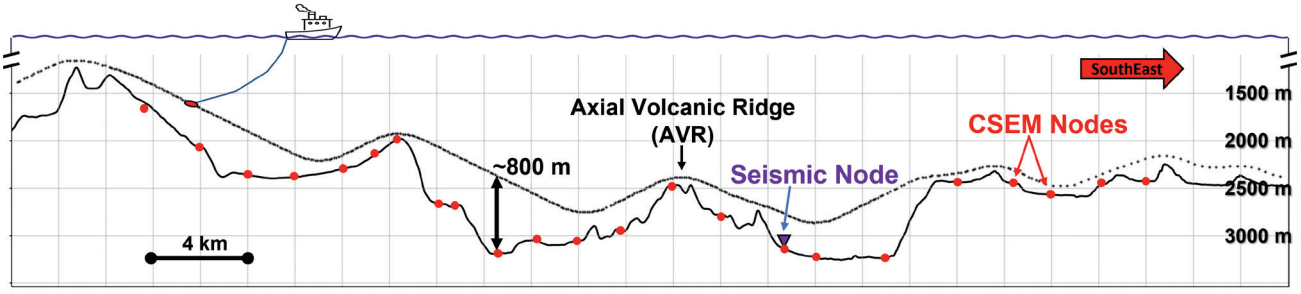

Figure 8 2D plot of the water bottom along Line 1 showing the locations of the 23 CSEM nodes, EM source positions and the location of the single seismic node.

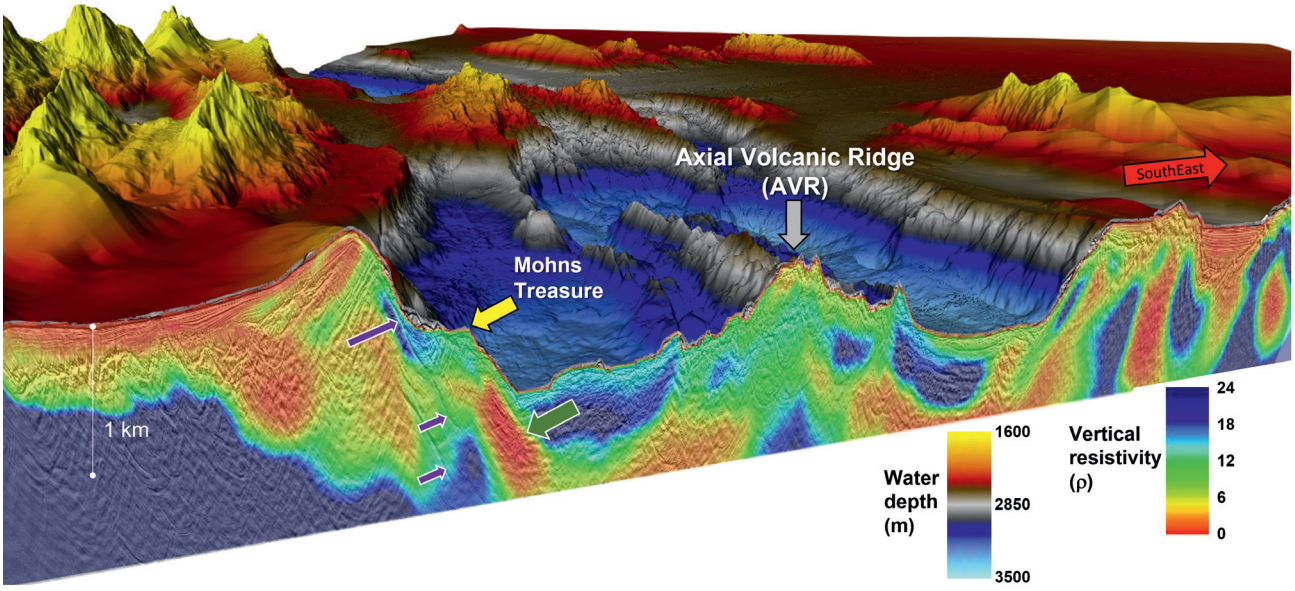

Figure 9 Vertical resistivity, seismic and bathymetry along Atlab-3 Line 1 viewed towards the north-east showing the AVR, the rift valleys on each side and Mohns Treasure on the western flank. Purple arrows identify faults and the green arrow a zone of low resistivity in close proximity to Mohns Treasure (yellow arrow).

imaged, showing that there are significant 3D effects at this location.

Summary

In this article, we have studied the use of 2D seismic and controlled source electromagnetic (CSEM) data to image the relatively shallow subsurface of the Mohns Ridge segment of the Arctic Mid-Ocean Ridge. Our objectives have been to compare the results of vintage and modern seismic acquisition and processing, to better understand the geological context of the region and to look at how the mineralised zone around Mohns Treasure is imaged on seismic and CSEM data with a view to further studies and future exploration.

All the results shown here, from both the seismic and CSEM acquisitions, are limited by being 2D, given the complex lateral variation in the sea bottom and subsurface. However, the imaging in the shallow sedimentary basins is good when modern processing and imaging technology is applied on both the Svalex and Atlab-3 data, with detailed layering and a broadband spectrum up to 100-200 Hz. The Atlab-3 data benefits from better wavelet control compared to the Svalex data, due to the near-field hydrophones and dual-sensor acquisition. Despite its much smaller source and shorter source-receiver offsets, it achieves similar signal strength and penetration. To obtain a true imaging of the 3D structures a full 3D acquisition is needed, but even this may not be adequate to detect the relatively small SMS deposits based on the seismic signatures. A future option might be a combination of a sparse layout of a grid of seismic nodes combined with 3D Ultra-High-Resolution imaging as described in, for example, MacGregor et al. (2019) and applied in igneous marine settings, as described in Planke et al. (2023). This combination would potentially achieve both shallow high-resolution imaging and deeper penetration and could be deployed in future initiatives to explore the seabed for mineral deposits.

The combined seismic and CSEM results provide subsurface indications for the mineralised zone around Mohns Treasure, as demonstrated by the coinciding zones of low resistivity (i.e., high conductivity) and faulting (Figure 9). This represents a step in understanding how the geological context of SMS bodies in this region can be imaged and which geophysical tools would be appropriate for exploration. In potential future regional exploration for SMS deposits, these tools may help to constrain geographically limited areas to be explored by manned or unmanned submersibles or by dredging.

Acknowledgements

We thank the ATLAB consortium (ABP Norway, Allton, EMGS, Equinor, InApril, Norce, NTNU, OFG, OD, PGS, Shearwater and TGS) and its coordinator Ståle Emil Johansen for cooperation and fruitful discussions throughout the Atlab-3 project period from August 2022 until the present day. We are also grateful to the staff of InApril for providing detailed information about the seismic node and Green Minerals for providing the Svalex data. We would also like to thank our colleague Paul Soundy for preparing Figures 1 and 2, and Sara Pink-Zerling, Sam Gray and Junior Potgieter for careful review of the manuscript and finally CGG Earth Data for funding this work.

References

Bruvoll, V., Breivik, A.J., Mjelde, R. and Pedersen, R.B. [2009]. Burial of the Mohn-Knipovich seafloor spreading ridge by the Bear Island Fan: Time constraints on tectonic evolution from seismic stratigraphy, *Tectonics*, **28**, TC4001, DOI: https://doi.org/10.1029/2008TC002396.

Buck, W.R., Lavier, L.L. and Poliakov, A.N.B. [2005]. Modes of faulting at mid-ocean ridges. *Nature*, 434, 719-723.

Canales, J.P. and Escartín, J. (conveners) [2010]. Detachments in Oceanic Lithosphere: Deformation, Magmatism, Fluid Flow and Ecosystems. *Chapman Conference Report*, Agros, Cyprus. https://usoceandiscovery.org/wp-content/uploads/2016/05/OCCWorkshopFinalReport.pdf.

Edmonds, H.N. et al. [2003]. Discovery of abundant hydrothermal venting on the ultraslow-spreading Gakkel ridge in the Arctic Ocean. *Nature,* **421**, 252-256.

German, C.R., Petersen. S. and Hannington, M.D. [2016]. Hydrothermal exploration of mid-ocean ridges: where might the largest sulfide deposits be forming?, *Chemical Geology,* **420**, 114-126.

Gallardo, L.A. and Meju, M.A. [2003]. Characterization of heterogeneous near-surface materials by joint 2D inversion of dc resistivity and seismic data. *Geophys. Res. Lett.*, **30**, 1658.

Hannington, M.D., Jamieson, J., Monecke, M., Petersen, S. and Beaulieu S. [2011]. The abundance of seafloor massive sulfide deposits, *Geology*, **39**, 1155-1158.

Johansen, S.E., Panzner, M., Mittet, R., Amundsen, H.E.F., Lim, A., Vik, E., Landrø, M. and Arntzen, B. [2019]. Deep electrical imaging of the ultraslow-spreading Mohns Ridge. *Nature,* **567**, 379-383 DOI: https://doi.org/10.1038/s41586-019-1010-0.

Lim, A., Brönner, M., Johansen, S.E. and Dumais, M.-A. [2019]. Hydrothermal activity at the ultraslow-spreading Mohns Ridge: new insights from near-seafloor magnetics. *Geochemistry, Geophysics, Geosystems,* **20**, 5691-5709. DOI: https://doi.org/10.1029/2019GC008439

MacGregor, L., Scott, L., Cooper, R. and Nicholls, J. [2022]. Ultra-High Resolution Seismic: Applications of P-Cable in the Energy Transition. *First Break*, **40**(11), 67-70. DOI: https://doi.org/10.3997/1365-2397.fb2022096.

Murton, B.J. et al. [2019]. Geological fate of seafloor massive sulphides at the TAG hydrothermal field (Mid-Atlantic Ridge). *Ore Geology Reviews*, 107, 903-925. DOI: https://doi.org/10.1016/j.oregeorev.2019.03.005.

Pedersen, R.B., Thorseth, I.H., Nygård, T.E., Lilley, M.D. and Kelley, D.S. [2010]. Hydrothermal activity at the Arctic mid-ocean ridges. *In: Rona, P.A., Devey, C.W., Dyment, J. and Murton, B.J. (eds.) Diversity of Hydrothermal Systems on Slow Spreading Ocean Ridges. American Geophysical Union Geophysical Monograph Series*, **188**, 67-89.

Planke, S., Lebedeva-Ivanova, N., Bünz, S., Binde, C., Berndt, C., Faleide, J.I., Huismans, R., Zastrozhnov, D., Manton, B., Stokke, H. and Betlem, P. [2023]. High-Resolution Core-Log-Seismic Integration and Igneous Seismic Geomorphology of IODP Expedition 396 Sites on the Mid-Norwegian Margin. In *NSG2023 29th European Meeting of Environmental and Engineering Geophysics* (Vol. 2023, **1**, 1-5). European Association of Geoscientists & Engineers.

Press Release [2023]. https://www.regjeringen.no/en/aktuelt/the-government-is-facilitating-a-new-ocean-industry-seabed-mineral-activities/id2985941/.

Ressursvurdering havbunnsmineraler [2023]. Ministry of Petroleum and Energy. Ressursvurdering havbunnsmineraler (npd.no). https://www.npd.no/globalassets/1-npd/fakta/havbunnsmineraler/publikasjoner/2023/ressursvurdering-havbunnsmineraler-20230127.pdf

Scholl, C., Hallinan, S., Watts, M.D. and Mirorelli, F. [2017]. Geological consistency from inversions of geophysical data. *79th EAGE Annual Meeting, Abstracts*, DOI: https://doi.org/10.3997/2214-4609.201700849.

Scholl, C., and Miorelli, F. [2019]. Airborne EM inversion on vertically unstructured model grids. *Exploration Geophysics*, DOI: https://doi.org/10.1080/08123985.2019.1668239.

Talwani, M. and Eldholm, O. [1977]. Evolution of the Norwegian-Greenland sea, *Geol. Soc. Am. Bull.*, **88**, 969-999, DOI: https://doi.org/10.1130/0016-7606(1977)88%3C969:EOTNS%3E2.0.CO;2.